# An unexpected organometallic intermediate in surface-confined Ullmann coupling†

Gianluca Galeotti, ‡[a,b] Marco Di Giovannantonio, §‡[a] Andrew Cupo, [c] Sarah Xing,[d] Josh Lipton-Duffin, [e] Maryam Ebrahimi, ¶[b] Guillaume Vasseur,[d] Bertrand Kierren,[d] Yannick Fagot-Revurat, [d] Damien Tristant,[c] Vincent Meunier, [c] Dmitrii F. Perepichka, [f] Federico Rosei *[b,g] and Giorgio Contini *[a,h]

Ullmann coupling or, more generally, dehalogenative aryl–aryl coupling, is one of the most widely exploited chemical reactions to obtain one- and two-dimensional polymers on metal surfaces. It is generally described as a two-step reaction: (i) dehalogenation, resulting in the formation of a stable intermediate organometallic phase and subsequent (ii) C–C coupling. The topology of the resulting polymer depends on the number and positions of the halogen atoms in the haloaromatic precursor, although its orientation and order are determined by the structure of the intermediate phase. Hitherto, only one intermediate structure, identified as an organometallic (OM) phase, has been reported for such a reaction. Here we demonstrate the formation of two distinct OM phases during the temperature-induced growth of poly(*para*-phenylene) from 1,4-dibromobenzene precursors on Cu(110). Beyond the already known linear-OM chains, we show that a phase reorganization to a chessboard-like 2D-OM can be activated in a well-defined temperature range. This new intermediate phase, revealed only when the reaction is carried out at low molecular coverages, was characterized by X-ray photoelectron spectroscopy, scanning tunneling microscopy and near-edge X-ray absorption fine structure spectroscopy, and modeled by density functional theory calculations. Our data show that the 2D-OM remains stable after cooling down the sample and is stabilized by four-Cu clusters at each node. The observation of such unexpected intermediate phase shows the complexity of the mechanisms underlying on-surface synthesis and broadens the understanding of Ullmann coupling, which continues to be astonishing despite its extensive use.

## Introduction

On-surface synthesis is an increasingly exploited bottom-up methodology to grow atomically precise nanostructures from carefully designed molecular precursors.[1,2] This approach relies on crystalline surfaces to support the low-dimensional growth of desired architectures through catalytically activated chemical reactions, and is capable of producing one- and two-dimensional (1D and 2D) organic arrays that are unlikely to occur naturally.[3–6] The achievement of covalent coupling between the building blocks is desirable, to ensure the mechanical and thermal stability of the atomically thin layer, and allows the extension of π-conjugation, which is the key aspect for using these materials in semiconducting devices.[7,8]

[a]*Istituto di Struttura della Materia, CNR, Via Fosso del Cavaliere 100, 00133 Roma, Italy. E-mail: giorgio.contini@cnr.it*
[b]*Centre Énergie, Matériaux et Télécommunications, Institut National de la Recherche Scientifique, 1650 Boulevard Lionel-Boulet, Varennes, QC, J3X 1S2, Canada. E-mail: rosei@emt.inrs.ca*
[c]*Department of Physics, Applied Physics and Astronomy, Rensselaer Polytechnic Institute, Jonsson-Rowland Science Center, 110 8th Street, Troy, NY 12180, USA*
[d]*Institut Jean Lamour, UMR 7198, Université de Lorraine, CNRS, F-54000 Nancy, France*
[e]*School of Chemistry, Physics and Mechanical Engineering, and Institute for Future Environments, Queensland University of Technology (QUT), 2 George Street, Brisbane, QLD 4001, Australia*
[f]*Department of Chemistry, McGill University, 801 Sherbrooke Street West, Montreal, QC H3A 0B8, Canada*
[g]*Institute of Fundamental and Frontier Sciences, University of Electronic Science and Technology of China, Chengdu 610054, P. R. China*
[h]*Department of Physics, University of Rome Tor Vergata, Via della Ricerca Scientifica 1, 00133 Roma, Italy*

†Electronic supplementary information (ESI) available: Fast-XPS observed phases, DFT calculations, structural models of phases, details of XPS peak analysis, XPS and STM comparison. See DOI: 10.1039/c9nr00672a

‡Equally contributing authors.

§Present addresses: Empa, Swiss Federal Laboratories for Materials Science and Technology, nanotech@surfaces Laboratory, Überlandstrasse 129, 8600 Dübendorf, Switzerland.
¶Present addresses: Physics Department E20, Technical University of Munich, James-Franck-Str. 1, D-85748 Garching, Germany.

In this framework, the formation of polymers is initiated by energetic input, either by annealing the surface or by light irradiation, according to the specific functional groups involved in the reaction. Changing the precursors, *i.e.* the building blocks, allows the modification of the structure and properties of the polymer.[5] Various chemical reactions have been used for carrying out on-surface polymerization.[1,9–13] Among these, Ullmann coupling has been the most successful for its generality, excellent regio- and chemo-selectivity, and convenient activation temperature (in the 100–300 °C range).[1,2,12,14–16] Using different halogens as leaving groups, a hierarchical growth of polymer architectures of increased complexity and/or an enhanced order can be achieved.[12,14,17]

Ullmann coupling[18] is generally understood as a two-step reaction, involving the formation of organo-cuprate intermediates (R-Cu-R) in the first step, with subsequent ejection of the metal to form covalently linked products in the second step.[19–21] On crystalline metal surfaces, the reaction has been proven to proceed in a similar manner.[9,15,22–25] Aside from the classical case of copper substrates,[26–28] on-surface coupling of aryl-halides has also been demonstrated on Ag and Au surfaces.[29–31] Stable organometallic (OM) phases are commonly observed on Cu and Ag,[28,32,33] while they are less frequent – but still reported – on Au.[34–38] Extensive studies of on-surface Ullmann coupling have been performed, exploring the effects of the detached halogen atoms,[25] the underlying surface,[29] and other reaction parameters,[17,32,39,40] although most focused on the final product (the polymer). However, the reaction pathways may proceed through the formation of other phases, *i.e.* intermediate products, with unique chemical and structural features. A successful case-study of the on-surface Ullmann reaction is the coupling of *para*-dihalobenzenes, characterized by linear-OM chains of substrate-stabilized phenyls, which shrink to poly(*para*-phenylene) (PPP) polymers after annealing.[15,24,25,33,41–43] Here we report the observation of an additional intermediate phase characterized by a 2D chessboard-like appearance during the Ullmann coupling of 1,4-dibromobenzene (dBB) on Cu(110). Using scanning tunneling microscopy (STM) and photoelectron spectroscopies, complemented with density functional theory (DFT) calculations we show that this structure is formed in an intermediate temperature range between the previously known linear-OM and the polymer phase, and is observed only for sub-monolayer surface coverage (≤0.6 ML) of the starting precursor.

## Results

When deposited on Cu(110) at room temperature (RT) under ultra-high vacuum (UHV) conditions, dBB molecules dehalogenate and form linear-OM chains that can be subsequently converted into a 1D polymer upon further annealing.[15] Fast-X-ray photoelectron spectroscopy (fast-XPS) maps at the C 1s core level acquired during temperature ramping of samples with different initial molecular coverages are reported in Fig. 1a. The chemical shift associated with the polymerization transition is observed in all the maps in the 190–200 °C range, where the C–C covalent coupling takes place (yellow line in Fig. 1a).[15,16,25] However, an additional shift is also present at lower temperature in the maps with initial coverage up to 0.6 ML (cyan line in Fig. 1a). To understand the origin of this unexpected reaction, we focused on the sample with an initial molecular coverage of 0.5 ML. Here, the two observed chemical shifts give rise to three distinct spectral features of the corresponding fast-XPS, each arising from the dominant phase in distinct temperature ranges (Fig. S1† and Discussion).[15,24] The first phase is dominant in the RT–145 °C range, the second in the 145–200 °C range, and the third above 200 °C (Fig. 1b). STM images, acquired after sequential annealing steps at increasing temperatures, reveals that the spectral features correspond to three morphologically distinct phases. At RT, the known linear-OM phase is present on the Cu(110) surface (Fig. 1c).[15] After annealing at 170 °C, a new phase is observed, characterized by rectangular symmetry, which we identify as the 2D-OM phase (Fig. 1e). The 2D-OM is converted into 1D polymers after annealing at 230 °C (Fig. 1g). Fig. 1d and f show the STM images of the surface after annealing at 145 °C and 200 °C, respectively, where the coexistence of two phases is observed. The 2D-OM phase is stable when the sample is cooled down to 5 K, as observed in STM images (Fig. 1d–f).

STM images of the 2D-OM phase reveal a chessboard-like motif forming distinct domains (*e.g.* blue box in Fig. 2a), separated by domain boundaries (blue arrow in Fig. 2a). The domain unit cell is described by the epitaxy matrix $(3, 2|-3, 2)$ (red box in Fig. 2a). The average domain size obtained from large-area STM images is 3 × 4 unit cells, with a maximum observed size of 6 × 6. Performing d$I$/d$V$ conductance mapping of a region where both linear- (green arrow in Fig. 2b and c) and 2D-OM phases are observed unveils that the domain boundaries (blue arrows in Fig. 2) exhibit spectroscopic characteristics identical to those of the linear-OM phase (Fig. 2c). As previously reported,[15] the linear-OM phase consists of phenyl rings anchored on either side to Cu atoms, which appear significantly brighter than the phenyls when imaged by STM. In the 2D-OM domain boundaries, we observe the same morphology, and as such we ascribe the bright protrusions to Cu atoms bridging phenyls (dark brown circles in Fig. 3a).

To understand the structure of the chessboard-like domains, we performed DFT calculations of several possible models (a detailed discussion is reported in section 2 of the ESI†). Fig. 3 shows the structure whose Tersoff–Hamann[44] STM simulation best matches the experimental data. This model comprises an array of four Cu adatoms at the nodes (Fig. 3a, orange circles) and phenyls as linkers, with Cu–Ph–Cu connections oriented along the $[1, -1, \pm1]$ directions. The distance between two copper atoms bridged by a phenyl is 0.7 nm. This value makes the Cu adatom clusters preferred anchoring sites for phenyl biradicals in the 2D-OM phase. Here, each Cu atom is linked to just one phenyl, rather than two as in the linear-OM, which plausibly explains the spectral differences observed in Fig. 2c. The features observed at the vertices of the unit cell are ascribed to Br atoms (Fig. 3a,

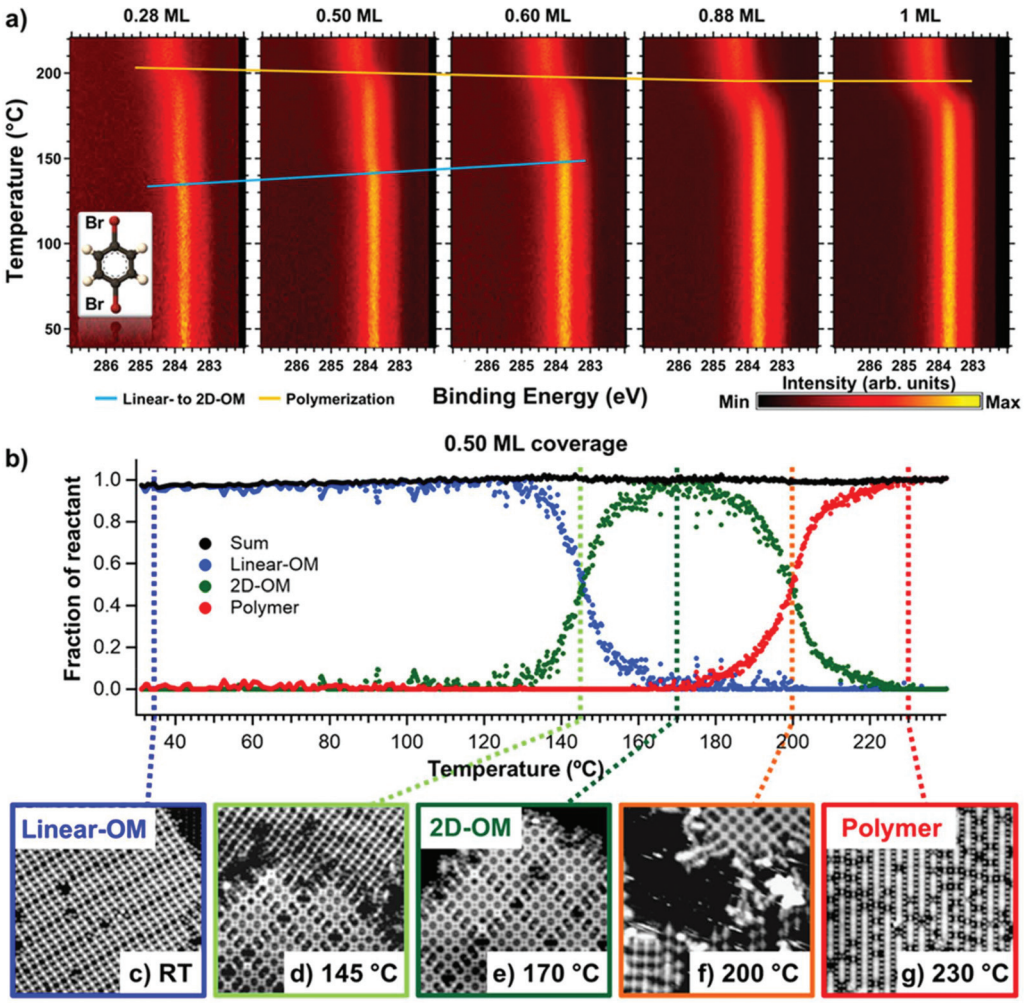


**Fig. 1** (a) C 1s fast-XPS maps of dBB on Cu(110) at different molecular coverages, from 0.28 ML to 1 ML. (b) Kinetic curves extracted from the fast-XPS map at 0.5 ML coverage according to a previously reported fitting procedure.[24] These curves represent the surface density of the different phases present on the surface as a function of temperature (see section 1 of the ESI†). (c–g) STM images (18 × 18 $nm^2$) of the sample with 0.5 ML coverage annealed at different temperatures, showing the phase evolution from linear-OM, to 2D-OM, to the polymer.

red circles).[15,25] These bromine atoms do not always fill the empty space of the network, as indicated by the black arrow in Fig. 2a. Cartoon models of the 2D-OM phase including the domain boundaries are shown in Fig. S4 and S5,† showing that Br atoms in the domain boundaries are located in the short-bridge position (Fig. S5†), in agreement with the linear-OM phase.[15,25]

As mentioned, we do not observe the 2D-OM phase for coverages greater than 0.6 ML (Fig. 1a). Based on the proposed model, the areal density of aromatic rings in the linear-OM, 2D-OM, and polymer phase is 2.0, 1.8, and 2.3 phenyls per $nm^2$, respectively (see Fig. S6†), and notably the density of the 2D-OM phase is lower than that of the linear-OM. If the coverage is close to 1 ML (above 0.90 ML for a 10% change in density, in agreement with the 0.88 ML experimental point), there is insufficient space on the surface for the expansion required for transformation into 2D-OM domains, and thus the conversion to the polymer occurs directly. The linear- to 2D-OM transition temperature increases as a function of initial coverage, while the 2D-OM to polymer transition temperature decreases; these trends can probably be connected to the different surface mobility of the phenyls in the linear-OM and 2D-OM phases. A higher surface temperature is needed to obtain the 2D-OM from the linear-OM. This can presumably be ascribed to (i) a higher surface density of Cu adatoms and (ii) their lower diffusion barrier, explaining the easier access to the 2D-OM phase, bearing a larger adatom-to-phenyl ratio. The fast-XPS shows that the 2D-OM phase is the most favorable phase at about 170 °C, while the STM shows that it is thermodynamically stable even at RT or at 5 K. In fact, we never observed a spontaneous reversion over a period of 3 days. To further characterize the newly observed 2D-OM phase, we performed spectroscopic investigations of the surfaces prepared at RT, and annealed to 170 °C and 230 °C, *via* XPS and C K-edge near-edge X-ray absorption fine structure (NEXAFS) spectroscopy (Fig. 4). XPS spectra acquired at the C 1s core

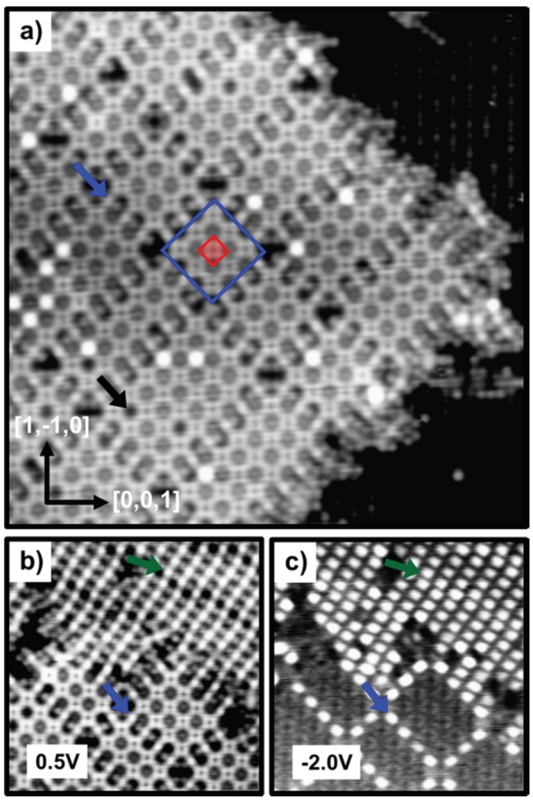


**Fig. 2** (a) STM image (22 × 22 nm$^2$) of the 2D-OM phase at 0.5 ML coverage of dBB on Cu(110) after annealing at 170 °C. The red box indicates the unit cell of a 2D-OM domain (blue box). The linear structures along the [1, −1, 0] direction are Br atoms adsorbed on the substrate. (b and c) STM image (14 × 14 nm$^2$) and corresponding conductance map (acquired at $V_b$ = −2.0 eV) of coexisting linear- and 2D-OM phases, showing the same spectroscopic features characterizing the 2D-OM domain boundaries and the linear-OM phase.

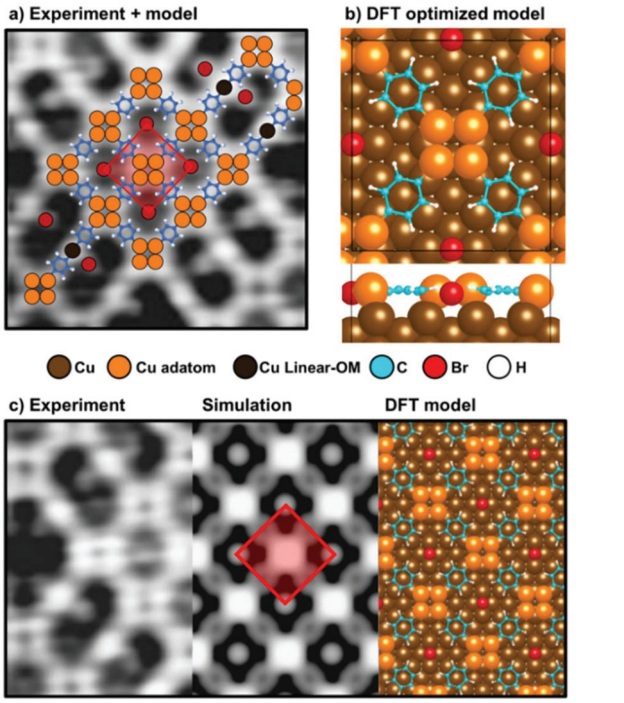


**Fig. 3** (a) STM image (5 × 5 nm$^2$) superimposed with the proposed structure of the 2D-OM phase and the domain boundary region. (b) Top and side views of DFT optimization of the 2D-OM structure. (c) Side-by-side view of the experimental area (4 × 3 nm$^2$), DFT simulated STM images at −2.0 V bias and DFT model. The red boxes in panels (a) and (c) indicate the unit cell of the 2D-OM network.

level for the linear-OM and polymer phases (at RT and 230 °C, respectively) show the same line shapes as previously reported.[15] The red and green components correspond to the four hydrogen terminated carbons, with the splitting probably arising to either a different position of the C–H bonds relative to the Cu lattice sites, or to vibrational modes, due to stretching type vibrations along the C–H bonds.[15,16] The blue component at 283.3 eV is due to the Ph–Cu–Ph type of linkage, typical of the linear-OM phase.[15,25] The small shoulder at low BE observed for the polymer phase arises from the C–Cu connections at the polymer endpoints, suggesting a predominance of short polymers. The C 1s spectrum of the 2D-OM phase (middle panel of Fig. 4a) shows a new feature that is not observed in neither the linear-OM nor the polymer spectra. While the red and green components likely have the same origin described above, the component at 283.6 eV (magenta) can be assigned to phenyls linked to Cu adatom clusters (Ph–Cu) as proposed in the model (Fig. 3). The ratio 1 : 5 between the components at 283.3 eV and 283.6 eV in the XPS spectrum of the 2D-OM phase agrees with the average number of Ph–Cu–Ph and Ph–Cu linkages observed by STM, with the relative abundance of Ph–Cu–Ph being substantially reduced from linear-OM to 2D-OM, as in the latter case it only arises from the domain boundaries. The peak positions, full width at half maximum (FWHM), and relative abundance for the three phases are reported in Table S1 of the ESI.†

The NEXAFS spectra acquired from surfaces prepared at RT and 230 °C are in agreement with previously reported measurements for the linear-OM and polymer phase.[15,25] The spectrum acquired on the 2D-OM phase (middle panel in Fig. 4b) exhibits a $\pi_1$* intensity for s- and p-polarization ($\theta$ = 0° and $\theta$ = 90°, respectively) which is essentially unchanged from that of the RT structure, and reflects the mostly planar adsorption geometry of the aromatic rings with respect to the surface. The split of the $\pi$* transition into two components ($\pi_1$* and $\pi_2$*) is attributed to symmetry breaking in the ring (due to geometrical distortions) and/or to the newly formed electronic state composed of $\pi$ electron orbitals of the adsorbate and the 3d electronic states of the substrate, as observed for the RT phase.[45,46] In the case of the 2D-OM, the character of the $\pi_2$* state is likely very similar to that of the linear-OM, and geometric distortions of the phenyl ring are present in both calculated geometries.

## Discussion

Despite the large number of published studies on surface-confined Ullmann polymerization, our findings show that the

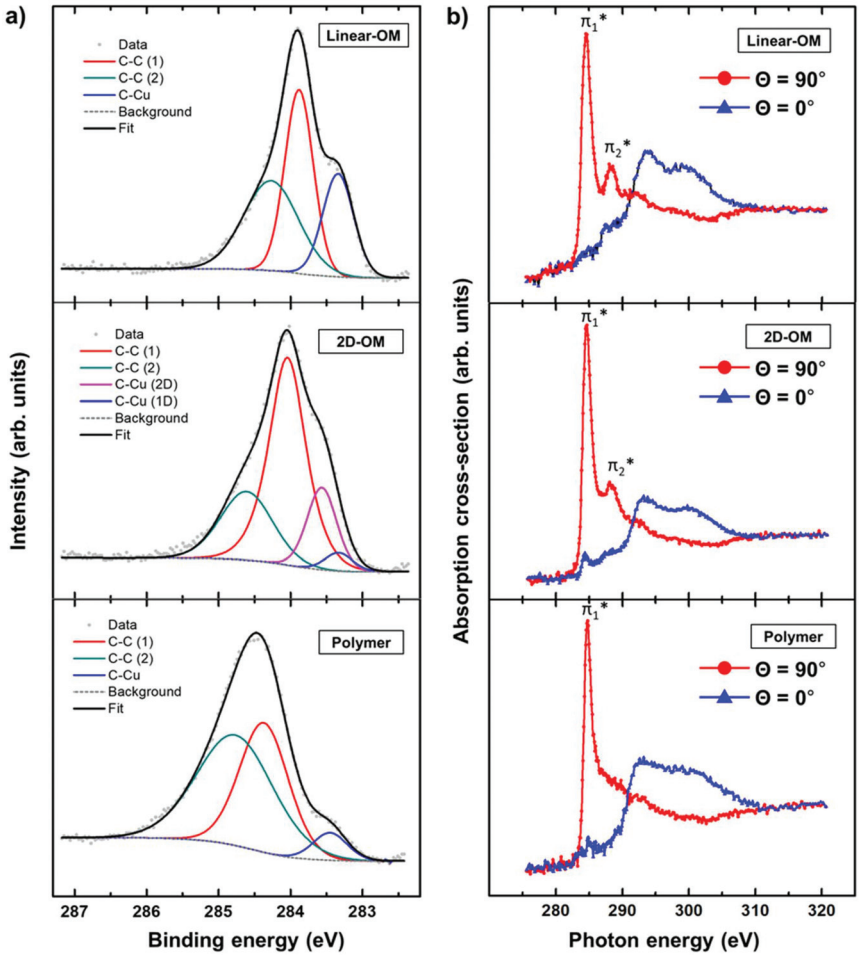


**Fig. 4** (a) Spectral deconvolution of C 1s XPS spectra of the three phases: linear-OM, 2D-OM and polymer. (b) Polarization-dependent C K-edge NEXAFS spectra of the linear-OM, 2D-OM and polymer phases measured at $\theta$ = 0° (s-polarization) and $\theta$ = 90° (p-polarization), respectively. For $\theta$ = 0°, the polarization vector of the incident polarized photons is on the surface along the [001] direction, while for $\theta$ = 90° the polarization vector is almost perpendicular to the surface.

complexity of its mechanistic pathways is not yet fully understood, even for the simplest precursor monomers. In particular, the observation of two distinct and stable OM phases (linear- and 2D-OM) is unusual given that no such result has yet been reported for this system[15,16,24,25,41] nor for systems using similar precursors.[25,26,28,33,42] To date, only linear (1D) OM phases have been reported for bidentate monomers, probably due to the narrow temperature and coverage ranges where additional 2D-OM phases might exist. Only a systematic study exploring the entire temperature range of interest and different starting molecular coverages is able to capture phases existing in a limited parameter space. Therefore, we do not exclude the fact that similar additional phases exist also for other molecule/substrate combinations. Another key aspect that characterizes our system is the presence of Cu clusters which stabilize the 2D-OM phase. Although the role of Cu clusters in homogeneous catalysis is well established,[47] in on-surface Ullmann coupling the stabilization of OM intermediates by metal clusters instead of single atoms has only been shown once, by Zhou *et al.*[48] Similarly to our case, they observed molecular aggregates where each (monoradical) molecule is stabilized by one metal atom.[48] However, these clusters were observed only for extremely low concentrations (0.1 ML of coverage), and, due to the mono-radical nature of the used precursor, did not yield an assembled structure. Differently, our 2D-OM phase represents an exceptional example of the extended ordered network.

Being able to control the self-assembly ordering and tessellation is a crucial aspect of supramolecular chemistry, which requires a deep understanding of molecular interactions for driving the system towards the wanted structure. It has been shown that the molecular ordering of intact halogenated molecules can be controlled by the temperature,[49,50] and that the tessellation of metal–organic self-assemblies can be controlled by changing the type of the metal.[51–54] However, the present work represents the first case of on-surface transition between two isomeric OM phases, driven solely by temperature. The behavior described herein could be of general interest: additional

stable ordered intermediates could also exist in the case of other reactions and systems, maybe in a short range of temperatures or for a precise set of parameters, and not experimentally observed so far. While enriching the fundamental understanding of the mechanism of the most important on-surface coupling reaction, our finding of multiple intermediates, with different molecular densities and dimensionality, could also have implications in the structural quality of the final polymers.[41] In fact, the presence of intermediate phases is an essential feature for the design of hierarchical on-surface polymerization, which is a key tool to improve the order and to control the dimensionality of the final polymer.[14,17,55] These later examples emphasize the importance of understanding the mechanisms of on-surface synthesis for the rational design of surface confined conjugated structures.

## Conclusion and perspectives

We report the observation of two structurally distinct intermediate phases in the Ullmann polymerization of dBB on Cu (110), created within well-defined temperature ranges. The already known linear-OM is converted into a 2D-OM chessboard-like structure. This phase has been observed during the annealing of the surface at a temperature between 145 °C and 200 °C for sub-monolayer surface coverage (≤0.6 ML) and remains stable after cooling down the sample to RT or below. Combining STM observations with DFT calculations, we have described the structural details of the 2D-OM phase, comprising phenyls bridging four-atom clusters of Cu adatoms. Investigations *via* XPS and NEXAFS support our findings and show that the presence of the 2D-OM phase and its evolution as a function of initial coverage cause slight differences in the polymerization temperature.

These results demonstrate that even for simple molecules, on-surface Ullmann coupling may follow multiple pathways. The observation of two stable OM phases, with distinct morphologies and spectroscopic fingerprints, shows the complexity of on-surface mechanisms, offering an opportunity for fine tuning the growth of specific structures through the design of different synthetic routes.

## Experimental section

All the experiments have been performed under UHV conditions (base pressures below $2 \times 10^{-10}$ mbar). The dBB precursor molecule (Sigma-Aldrich, 98% purity) is shown in Fig. 1 and was deposited onto Cu(110) (MaTecK GmbH) through a leak valve, while the substrate was held at RT. The Cu(110) surface was prepared before molecule deposition by multiple cycles of $Ar^+$ sputtering (0.8–1.2 keV) followed by annealing (480 °C). The surface coverage was evaluated by comparing the XPS C 1s/Cu 2p peak intensity ratio, imposing 1 ML in the case of saturated coverage.

STM was performed with an Omicron LT-STM at 5 K, using constant tunneling current (0.2 nA) and constant bias voltage measured from the tip to the sample (0.5 V, unless stated otherwise), at various surface coverages calibrated with an XPS spectrometer hosted in the same UHV chamber. The reported STM images correspond to 0.5 ML coverage, for a better comparison with the fast-XPS experiments. The d$I$/d$V$ maps were recorded in the open feedback loop mode ($V$ = 2 V) using a lock-in amplifier (peak to peak modulated voltage of 30 mV, $f$ = 1100 Hz). STM images were analyzed using WSxM,[56] and treated for line-by-line flattening, plane subtraction and contrast enhancement.

XPS, fast-XPS and NEXAFS were performed at the ALOISA beamline at the Elettra synchrotron radiation facility in Trieste (Italy). For XPS and fast-XPS experiments, a normal electron emission geometry was used, with the linearly polarized radiation having a 4° grazing incidence, by using a home-built hemispherical electron analyzer equipped with a multichannel plate (MCP) detector. The C 1s core level fast-XPS maps have been acquired using 390 eV of photon energy, while increasing the temperature of Cu(110) from RT to 230 °C (0.2 °C $s^{-1}$), by using a heating element located underneath the sample. Every line of the fast-XPS map is obtained from snapshots of the C 1s peak (one spectrum per second) at the reported temperature, with a PE of 30 eV and an overall energy resolution of 350 meV. A partial electron yield, obtained by using a channeltron with a −240 V biased filtering grid, was used to record the NEXAFS C K-edge spectra with a photon energy resolution of 100 meV. The photon energy was calibrated by measuring the drain current on the last refocusing mirror of the beamline simultaneously with the C K-edge. The C K-edge spectrum acquired from clean Cu(110) was used to normalize the spectra. Rotating the sample along the beam axis allowed performing polarization dependent measurements. The surface angle ($\theta$) was changed from transverse electric (TE, s-polarization) to transverse magnetic (TM, almost p-polarization) with respect to the polarization vector with the grazing photon angle of incidence fixed at 6° (for details about photon energy calibration and NEXAFS geometry see the study by Floreano *et al.*).[57]

DFT calculations were performed using the Vienna *Ab initio* Simulation Package (VASP).[58] To include non-local interactions (in particular between the Cu surface and the carbon structure), the optB86b-vdW exchange correlation functional was implemented.[59–61] An energy cutoff of 400 eV was used with projector-augmented wave pseudopotentials.[62] Given the large size of the unit cell, a gamma-point $k$-point sampling was set for all calculations. A vacuum spacing of ∼15 Å was used to prevent interactions between periodic images. Atomic coordinates were relaxed to a force cutoff of 0.01 eV $Å^{-1}$. The Cu(110) substrate was represented by six layers, with the bottom four layers fixed. The STM image simulations were carried out within the Tersoff–Hamann approximation.[44] Atomic models were visualized with VESTA.[63] For the case reported in Fig. S2a,† the PBE functional[64] was used with the D3 method to include van der Waals interactions,[65] and the Cu(110) substrate consisted of nine layers with the bottom five fixed in the calculations.

## Conflicts of interest

There are no conflicts to declare.

## Acknowledgements

This work is partially supported by a project Grande Rilevanza Italy-Quebec of the Italian Ministero degli Affari Esteri e della Cooperazione Internazionale (MAECI), Direzione Generale per la Promozione del Sistema Paese and the Italy-France International Program of Scientific Cooperation (PICS CNR-CNRS). G. C. and F. R. acknowledge support from CNR through Short-term Mobility (STM) Fellowships. The authors acknowledge beamtime access and support from Elettra Light Source in Italy, and thank Luca Floreano, Alberto Verdini and Albano Cossaro for their help and guidance during the synchrotron measurements. G. G and G. C. thank Nicola Zema for laboratory support and useful discussions. F. R. and D. F. P. are supported by NSERC through individual Discovery Grants as well as by an FRQNT team grant. F. R. is also grateful to the Canada Research Chair program for funding and partial salary support. A. C. was supported by NSF Grant EFRI 2-DARE (EFRI-1542707) and supercomputing resources were provided by the Center for Computational Innovations (CCI) at Rensselaer Polytechnic Institute. D. T. acknowledges support from the Office of Naval Research.

## Notes and references

1 A. Gourdon, *On-Surface Synthesis*, Springer International Publishing, 2016.
2 D. G. De Oteyza and C. Rogero, *On-Surface Synthesis II*, Springer International Publishing, 2018.
3 A. K. Geim and K. S. Novoselov, *Nat. Mater.*, 2007, **6**, 183–191.
4 F. Rosei, *J. Phys.: Condens. Matter*, 2004, **16**, S1373.
5 D. F. Perepichka and F. Rosei, *Science*, 2009, **323**, 216–217.
6 M. El Garah, J. M. MacLeod and F. Rosei, *Surf. Sci.*, 2013, **613**, 6–14.
7 R. Gutzler and D. F. Perepichka, *J. Am. Chem. Soc.*, 2013, **135**, 16585–16594.
8 L. Cardenas, R. Gutzler, J. Lipton-Duffin, C. Fu, J. L. Brusso, L. E. Dinca, M. Vondráček, Y. Fagot-Revurat, D. Malterre and F. Rosei, *Chem. Sci.*, 2013, **4**, 3263–3268.
9 M. Xi and B. E. Bent, *J. Am. Chem. Soc.*, 1993, **115**, 7426–7433.
10 J. Liu, P. Ruffieux, X. Feng, K. Mullen and R. Fasel, *Chem. Commun.*, 2014, **50**, 11200–11203.
11 M. Di Giovannantonio, T. Kosmala, B. Bonanni, G. Serrano, N. Zema, S. Turchini, D. Catone, K. Wandelt, D. Pasini, G. Contini and C. Goletti, *J. Phys. Chem. C*, 2015, **119**, 19228–19235.
12 M. Di Giovannantonio and G. Contini, *J. Phys.: Condens. Matter*, 2018, **30**, 093001.
13 R. Lindner and A. Kühnle, *ChemPhysChem*, 2015, **16**, 1582–1592.
14 L. Lafferentz, V. Eberhardt, C. Dri, C. Africh, G. Comelli, F. Esch, S. Hecht and L. Grill, *Nat. Chem.*, 2012, **4**, 215–220.
15 M. Di Giovannantonio, M. El Garah, J. Lipton-Duffin, V. Meunier, L. Cardenas, Y. Fagot Revurat, A. Cossaro, A. Verdini, D. F. Perepichka, F. Rosei and G. Contini, *ACS Nano*, 2013, **7**, 8190–8198.
16 M. Di Giovannantonio, M. El Garah, J. Lipton-Duffin, V. Meunier, L. Cardenas, Y. Fagot-Revurat, A. Cossaro, A. Verdini, D. F. Perepichka, F. Rosei and G. Contini, *ACS Nano*, 2014, **8**, 1969–1971.
17 J. Eichhorn, D. Nieckarz, O. Ochs, D. Samanta, M. Schmittel, P. J. Szabelski and M. Lackinger, *ACS Nano*, 2014, **8**, 7880–7889.
18 F. Ullmann and J. Bielecki, *Ber. Dtsch. Chem. Ges.*, 1901, **34**, 2174–2185.
19 P. E. Fanta, *Synthesis*, 1974, 9–21.
20 T. Cohen and I. Cristea, *J. Am. Chem. Soc.*, 1976, **98**, 748–753.
21 C. Sambiagio, S. P. Marsden, A. J. Blacker and P. C. McGowan, *Chem. Soc. Rev.*, 2014, **43**, 3525–3550.
22 J. Björk, F. Hanke and S. Stafström, *J. Am. Chem. Soc.*, 2013, **135**, 5768–5775.
23 M. Lackinger, *Chem. Commun.*, 2017, **53**, 7872–7885.
24 M. Di Giovannantonio, M. Tomellini, J. Lipton-Duffin, G. Galeotti, M. Ebrahimi, A. Cossaro, A. Verdini, N. Kharche, V. Meunier, G. Vasseur, Y. Fagot-Revurat, D. F. Perepichka, F. Rosei and G. Contini, *J. Am. Chem. Soc.*, 2016, **138**, 16696–16702.
25 G. Galeotti, M. Di Giovannantonio, J. Lipton-Duffin, M. Ebrahimi, S. Tebi, A. Verdini, L. Floreano, Y. Fagot-Revurat, D. F. Perepichka, F. Rosei and G. Contini, *Faraday Discuss.*, 2017, **204**, 453–469.
26 M. M. Blake, S. U. Nanayakkara, S. A. Claridge, L. C. Fernández-Torres, E. C. H. Sykes and P. S. Weiss, *J. Phys. Chem. A*, 2009, **113**, 13167–13172.
27 J. A. Lipton-Duffin, J. A. Miwa, M. Kondratenko, F. Cicoira, B. G. Sumpter, V. Meunier, D. F. Perepichka and F. Rosei, *Proc. Natl. Acad. Sci. U. S. A.*, 2010, **107**, 11200–11204.
28 W. Wang, X. Shi, S. Wang, M. A. Van Hove and N. Lin, *J. Am. Chem. Soc.*, 2011, **133**, 13264–13267.
29 M. Bieri, M. T. Nguyen, O. Groning, J. M. Cai, M. Treier, K. Ait-Mansour, P. Ruffieux, C. A. Pignedoli, D. Passerone, M. Kastler, K. Mullen and R. Fasel, *J. Am. Chem. Soc.*, 2010, **132**, 16669–16676.
30 K. A. Simonov, A. V. Generalov, A. S. Vinogradov, G. I. Svirskiy, A. A. Cafolla, C. McGuinness, T. Taketsugu, A. Lyalin, N. Mårtensson and A. B. Preobrajenski, *Sci. Rep.*, 2018, **8**, 3506.
31 H. Zhang, H. Lin, K. Sun, L. Chen, Y. Zagranyarski, N. Aghdassi, S. Duhm, Q. Li, D. Zhong, Y. Li, K. Müllen, H. Fuchs and L. Chi, *J. Am. Chem. Soc.*, 2015, **137**, 4022–4025.
32 L. Dong, S. Wang, W. Wang, C. Chen, T. Lin, J. Adisoejoso and N. Lin, in *On-Surface Synthesis*, Springer, 2016, pp. 23–42.

33 J. Lipton-Duffin, O. Ivasenko, D. Perepichka and F. Rosei, *Small*, 2009, **5**, 592–597.
34 L. Grill, M. Dyer, L. Lafferentz, M. Persson, M. V. Peters and S. Hecht, *Nat. Nanotechnol.*, 2007, **2**, 687–691.
35 S. Schlögl, W. M. Heckl and M. Lackinger, *Surf. Sci.*, 2012, **606**, 999–1004.
36 K. A. Simonov, N. A. Vinogradov, A. S. Vinogradov, A. V. Generalov, E. M. Zagrebina, N. Mårtensson, A. A. Cafolla, T. Carpy, J. P. Cunniffe and A. B. Preobrajenski, *J. Phys. Chem. C*, 2014, **118**, 12532–12540.
37 M. Di Giovannantonio, O. Deniz, J. I. Urgel, R. Widmer, T. Dienel, S. Stolz, C. Sánchez-Sánchez, M. Muntwiler, T. Dumslaff, R. Berger, A. Narita, X. Feng, K. Müllen, P. Ruffieux and R. Fasel, *ACS Nano*, 2018, **12**, 74–81.
38 M. Lischka, M. Fritton, J. Eichhorn, V. S. Vyas, T. Strunskus, B. V. Lotsch, J. Björk, W. M. Heckl and M. Lackinger, *J. Phys. Chem. C*, 2018, **122**, 5967–5977.
39 Q. Fan, J. M. Gottfried and J. Zhu, *Acc. Chem. Res.*, 2015, **48**, 2484–2494.
40 Q. Fan, T. Wang, J. Dai, J. Kuttner, G. Hilt, J. M. Gottfried and J. Zhu, *ACS Nano*, 2017, **11**, 5070–5079.
41 G. Vasseur, Y. Fagot-Revurat, M. Sicot, B. Kierren, L. Moreau, D. Malterre, L. Cardenas, G. Galeotti, J. Lipton-Duffin, F. Rosei, M. Di Giovannantonio, G. Contini, P. Le Fèvre, F. Bertran, L. Liang, V. Meunier and D. F. Perepichka, *Nat. Commun.*, 2016, **7**, 10235.
42 G. S. McCarty and P. S. Weiss, *J. Am. Chem. Soc.*, 2004, **126**, 16772–16776.
43 G. McCarty and P. Weiss, *J. Phys. Chem. B*, 2002, **106**, 8005–8008.
44 J. Tersoff and D. R. Hamann, *Phys. Rev. B: Condens. Matter Mater. Phys.*, 1985, **31**, 805–813.
45 J. L. Solomon, R. J. Madix and J. Stöhr, *Surf. Sci.*, 1991, **255**, 12–30.
46 J. Stöhr, *NEXAFS spectroscopy*, Springer-Verlag, Berlin Heidelberg, 1992.
47 G. Suss-Fink and G. Meister, in *Advances in Organometallic Chemistry*, ed. F. G. A. Stone and R. West, Academic Press, 1993, vol. 35, pp. 41–134.
48 X. Zhou, C. Wang, Y. Zhang, F. Cheng, Y. He, Q. Shen, J. Shang, X. Shao, W. Ji, W. Chen, G. Xu and K. Wu, *Angew. Chem., Int. Ed.*, 2017, **56**, 12852–12856.
49 Q. Fan, L. Liu, J. Dai, T. Wang, H. Ju, J. Zhao, J. Kuttner, G. Hilt, J. M. Gottfried and J. Zhu, *ACS Nano*, 2018, **12**, 2267–2274.
50 C.-H. Shu, S.-Z. Zhang, C.-X. Wang, J.-L. Chen, Y. He, K.-J. Shi and P.-N. Liu, *Chem. Commun.*, 2018, **54**, 13670–13673.
51 A. Shchyrba, C. Wäckerlin, J. Nowakowski, S. Nowakowska, J. Björk, S. Fatayer, J. Girovsky, T. Nijs, S. C. Martens, A. Kleibert, M. Stöhr, N. Ballav, T. A. Jung and L. H. Gade, *J. Am. Chem. Soc.*, 2014, **136**, 9355–9363.
52 J. I. Urgel, D. Écija, G. Lyu, R. Zhang, C.-A. Palma, W. Auwärter, N. Lin and J. V. Barth, *Nat. Chem.*, 2016, **8**, 657.
53 D. Écija, J. I. Urgel, A. P. Seitsonen, W. Auwärter and J. V. Barth, *Acc. Chem. Res.*, 2018, **51**, 365–375.
54 L. Dong, Z. A. Gao and N. Lin, *Prog. Surf. Sci.*, 2016, **91**, 101–135.
55 C. Steiner, J. Gebhardt, M. Ammon, Z. Yang, A. Heidenreich, N. Hammer, A. Görling, M. Kivala and S. Maier, *Nat. Commun.*, 2017, **8**, 14765.
56 I. Horcas, R. Fernandez, J. Gomez-Rodriguez, J. Colchero, J. Gómez-Herrero and A. Baro, *Rev. Sci. Instrum.*, 2007, **78**, 013705.
57 L. Floreano, A. Cossaro, R. Gotter, A. Verdini, G. Bavdek, F. Evangelista, A. Ruocco, A. Morgante and D. Cvetko, *J. Phys. Chem. C*, 2008, **112**, 10794–10802.
58 G. Kresse and J. Furthmüller, *Phys. Rev. B: Condens. Matter Mater. Phys.*, 1996, **54**, 11169–11186.
59 M. Dion, H. Rydberg, E. Schröder, D. C. Langreth and B. I. Lundqvist, *Phys. Rev. Lett.*, 2004, **92**, 246401.
60 G. Román-Pérez and J. M. Soler, *Phys. Rev. Lett.*, 2009, **103**, 096102.
61 J. Klimeš, D. R. Bowler and A. Michaelides, *Phys. Rev. B: Condens. Matter Mater. Phys.*, 2011, **83**, 195131.
62 P. E. Blöchl, *Phys. Rev. B: Condens. Matter Mater. Phys.*, 1994, **50**, 17953–17979.
63 K. Momma and F. Izumi, *J. Appl. Crystallogr.*, 2011, **44**, 1272–1276.
64 J. P. Perdew, K. Burke and M. Ernzerhof, *Phys. Rev. Lett.*, 1996, **77**, 3865–3868.
65 S. Grimme, J. Antony, S. Ehrlich and H. Krieg, *J. Chem. Phys.*, 2010, **132**, 154104.